Electronic Supplementary Information

Coordination engineering of single-atom Ruthenium in 2D MoS2 for enhanced hydrogen evolution

Dong Guo,[#a] Xiong-Xiong Xue,[#b] Menggai Jiao,[#c] Jinhui Liu,[#a] Tian Wu,[a] Xiandi Ma,[c] Die Lu,[c] Rui Zhang,[c] Shaojun Zhang,[a] Gonglei Shao*[c] and Zhen Zhou*[c]

[a] School of Materials Science and Engineering, Zhengzhou University, Zhengzhou 450001, P. R. China

[b] School of Physics and Optoelectronics, Xiangtan University, Xiangtan 411105, P. R. China

[c] Interdisciplinary Research Center for Sustainable Energy Science and Engineering (IRC4SE^2), School of Chemical Engineering, Zhengzhou University, Zhengzhou 450001, P. R. China

*Correspondence to: shaogonglei@zzu.edu.cn; zhenzhou@zzu.edu.cn

EXPERIMENTAL METHODS

Materials and reagents.

Molybdenum disulfide nanosheets (MoS_2), Ruthenium chloride ($RuCl_3$), hydrogen peroxide (H_2O_2), Lithium fluoride (LiF), Ammonium hydroxide ($NH_3 \cdot H_2O$), concentrated hydrochloric acid (HCl) and ethanol were purchased from the Sigma Shanghai Reagent Company, and used in experiments without further purification.

Synthesis of 2D Vs - MoS_2 nanosheets.

MoS_2 (480 mg) was placed into a beaker containing 300 ml of 5 mol L^{-1} H_2O_2 solution and then treated under ultrasonication for 60 s. The resulting mixture was then quickly transferred to a suction filtration unit. The Vs - MoS_2 obtained by suction filtration was washed with deionized water and freeze-drying before further processing.

Synthesis of 2D X - MoS_2 (X = O, N, F) nanosheets.

F - MoS_2 was synthesized using the immersion method. Initially, 1.297 g of LiF was added to a beaker containing 50 ml of water and 7.5 ml of HCl, facilitating complete dissolution through 10 min ultrasonic treatment. Subsequently, 80 mg of Vs - MoS_2 was added to the above solution, and the reaction was conducted under stirring conditions at room temperature for 48 h. The resulting F - MoS_2, obtained from the reaction, undergoes a series of post-synthesis procedures, including filtration, washing, and freeze-drying for further processing.

N - MoS_2 was prepared by the immersion method. 80 mg of Vs - MoS_2 was added to a beaker containing 50 ml of water and 3.33 ml of $NH_3 \cdot H_2O$, and the reaction was carried out under stirring conditions for 48 h. After the reaction concluded, N - MoS_2 was obtained through a series of

procedures, including filtration, washing, and freeze-drying.

O - MoS_2 was prepared by a two-step process involving oxygen plasma treatments. First, 160 mg of Vs - MoS_2 was spread flat in a glass petri dish and treated in the plasma chamber under 30 W for 60 s. Subsequently, the obtained powder was re-mixed and evenly spread for a second round of plasma treatment under the same conditions to obtain O - MoS_2.

Synthesis of 2D Ru - X - MoS_2 (X = O, N, F) nanosheets.

Ru - X - MoS_2 was prepared by the immersion method. Among then, 80 mg of X - MoS_2 was added into 50 mL of 10 mol L^{-1} $RuCl_3$ solution, and the reaction in this solution is conducted under stirring conditions at room temperature for 48 h. At the end of the reaction the samples were filtered and washed. The sample was finally annealed in a tube furnace at 200 °C for 2 h, under Ar atmosphere, to obtain Ru - X - MoS_2.

Characterization. The surface morphology of these 2D Ru - X - MoS_2 nanosheets was investigated using SEM (Hitachi-S4800). The X-ray diffraction (XRD) patterns were acquired using a Bruker Dimension Icon D8 Advance system, employing Cu Kα radiation at 40 kV and 40 mA. TGA data were taken using a thermal analysis equipment (NETZSCH STA449F3) in an Ar atmosphere with the temperature range from 50 °C to 800 °C and heating rate of 10 °C min^{-1}. A WITec alpha 300R spectrometer with a 532 nm laser excitation was used to get Raman spectra. The samples' elements and valence states were examined using ESCALAB 250Xi XPS with a monochromatic Al Kα source (λ = 1486.6 eV). Charging corrections was made using the adventitious C 1s peak of about 284.8 eV. ICP-OES was used to detect the contents of heterometals in different products by an Optima 7300 DV system.

HAADF-STEM pictures and energy dispersive X-ray spectroscopy (EDS) mapping studies were

carried out on the FEI Titan Cubed Themis G2 300 with a probe corrector and a monochromator at 200 kV.

The Ru K-edge XAFS investigations were carried out at the Shanghai Synchrotron Radiation Facility (SSRF)'s BL14W Beam line using Si(111) crystal monochromators. Before the beamline analysis, samples were put in aluminum sample containers and sealed with Kapton tape film. The XAFS spectra were acquired at ambient temperature using a 4-channel Silicon Drift Detector (SDD) Bruker 5040. In transmission mode, spectra of Ru K-edge extended X-ray absorption fine structure (EXAFS) were observed. There were no differences in the line form or peak position of Ru K-edge XANES spectra between two scans of the same sample. The acquired XAFS spectral data were processed in the Athena module of Demeter software (version 0.9.26) for background, leading and trailing edge line calibration. The acquired XAFS spectral data were processed in the Athena module of Demeter software (version 0.9.26) for background, leading and trailing edge line calibration.[1] Fourier transform fitting was then performed in the Artemis module of Demeter software (version 0.9.26).[1] The k^2 weighting, k ranging from 3 - 12 $Å^{-1}$, R ranging from 1 - 2.7 Å were used for the fitting of Ru - O - MoS_2. Wavelet transformation was implemented through Platform-Free Fortran (Hama Fortran version) developed by Harald Funke and Marina Chukalina. In the wavelet transform analysis, the $\chi(k)$ exported from Demeter software (Athena module) was imported into Hama Fortran version, using the following parameter list: R range is 0 - 4 Å, k range is 0 - 12 $Å^{-1}$; k weight is 2; The Morlet function is used as the mother wavelet, with $\kappa = 10$ and $\sigma = 1$ to provide the overall distribution.

Electrochemical measurements.

Electrochemical measurements were performed on a CHI 760E electrochemical station (CH

Instruments) using a standard three-electrode electrochemical cell at room temperature. H_2SO_4 solution (0.5 mol L^{-1}), phosphate buffered saline (1 mol L^{-1}) and KOH solution (1 mol L^{-1}) were used as acidic, neutral, and alkaline electrolytes, respectively. $Hg/HgCl_2$ electrode and Hg/HgO_2 electrode were used as reference electrode and graphite rod as counter electrode. Prior to each measurement, the working electrode was ground and polished three times with fine alumina powder and washed with distilled water to remove residual catalyst. The counter electrode was also washed with distilled water before use. Before the electrocatalytic measurements, 2 mg of sample, 0.2 mg of carbon black and 40 μL of Nafion solution were dispersed in 960 μL of ethanol by sonication to produce a homogeneous catalyst ink. Then, 20 μL of the catalyst ink was dropped onto a glassy carbon with a diameter of 3 mm as the working electrode. Linear scanning voltammetric (LSV) polarization curves were acquired at a scan rate of 5 mV s-1. Where all measured potentials with the reference electrode were transformed to reversible hydrogen electrode (RHE) according to the formula ($E_{RHE} = E_{SCE} + 0.0592 \times pH + 0.241$ V or $E_{RHE} = E_{Hg/HgO} + 0.059 \times pH + 0.098$ V). All overpotential values and Tafel slop values reported in the text were obtained from LSV curves corrected for iR. At room temperature, a standard three-electrode setup was used to conduct Cyclic voltammograms (CV) with varying scan rates (5, 10, 20, 40, 80, 160, and 250 mV s^{-1}). The double-layer capacitance (C_{dl}) values were calculated using Δj vs. v plots (where $\Delta j = (j_a - j_b)/2$). The electrochemically active surface area (ECSA) of the catalyst can be calculated by dividing the C_{dl} by the specific capacitance (C_S) of the sample, where Cs is typically in the range of 20-60 μF cm^{-2} for MoS_2 samples[2,3]. In our calculations, we assume 40 μF cm^{-2}. Faraday efficiency is the ratio of actual to theoretical hydrogen production. The current density was maintained at 10 mA cm^{-2} in acidic, neutral and alkaline electrolytes for 10 hours using Chronopotentiometry method, during which the hydrogen produced by the reaction was

collected through an inverted graduated cylinder. The hydrogen production was then recorded at 2 h, 4 h, 6 h, 8 h and 10 h. Electrochemical impedance spectroscopy (EIS) was measured at frequencies ranging from 0.1 Hz to 100 kHz. The electrochemical stability of these catalysts was evaluated using chronoamperometry method in acidic, neutral and alkaline electrolytes.

DFT calculations

All calculations were performed using the spin-polarized density functional theory, implemented in the Vienna Ab initio Simulation Package (VASP).[4,5] The exchange-correlation interaction is described by the Perdew-Burke-Ernzerhof (PBE) functionals with the generalized gradient approximation (GGA).[6] The projector augmented wave pseudopotential is adopted to describe nuclei-electron interactions. A cutoff energy of 450 eV with the plane wave basis set is used for all calculations and the energy and force convergence criteria are set to 10^{-5} eV and 0.02 eV $Å^{-1}$, respectively. The 5 × 5 × 1 single-layer MoS_2 supercell is employed to build Ru-doped MoS_2 models coordinated with various nonmetallic atoms. The 4 × 4 × 1 and 8 × 8 × 1 Monkhorst-Pack grids centered at the gamma (Γ) point are used to sample the Brillouin zone for geometries relaxed and electronic structure calculations, respectively. A 15 Å vacuum region was created along the z-direction to avoid the interaction between neighboring models under periodic boundary conditions.

The Gibbs free energy for hydrogen adsorption (ΔG_{H^*}) were calculated based on the model of computational hydrogen electrode and can be obtained by: [7,8]

$$\Delta G_{H^*} = \Delta E_{H^*} + \Delta E_{ZPE} - T\Delta S$$

where ΔE_{ZPE} and ΔS are the zero-point energy correction and the vibrational entropy change between the adsorbed hydrogen and hydrogen in the gas phase, respectively. ΔE_{H^*} is the hydrogen adsorption energy and is calculated by：

$$\Delta E_{H^*} = E_{H^*} - E_{surface} - 1/2E_{H_2}$$

where E_{H^*} and $E_{surface}$ represent the total energies of the surface model with an adsorbed H and the clear surface model, respectively. E_{H_2} is the energy of the hydrogen molecule in the gas-phase.

The d-band center (ε_d) of the Ru atom is calculated as follows:[6]

$$\varepsilon_d = \frac{\int_{-\infty}^{\infty} \rho_d(\varepsilon)\varepsilon d\varepsilon}{\int_{-\infty}^{\infty} \rho_d(\varepsilon) d\varepsilon}$$

where $\rho_d(\varepsilon)$ is the density of states projected onto the d orbital of the Ru atom and ε is the energy position of the d-orbital relative to the Fermi level. The d band center is calculated by integrating the entire d orbital based on the distribution of the d-projected density of states, which includes all of the occupied and unoccupied orbitals.

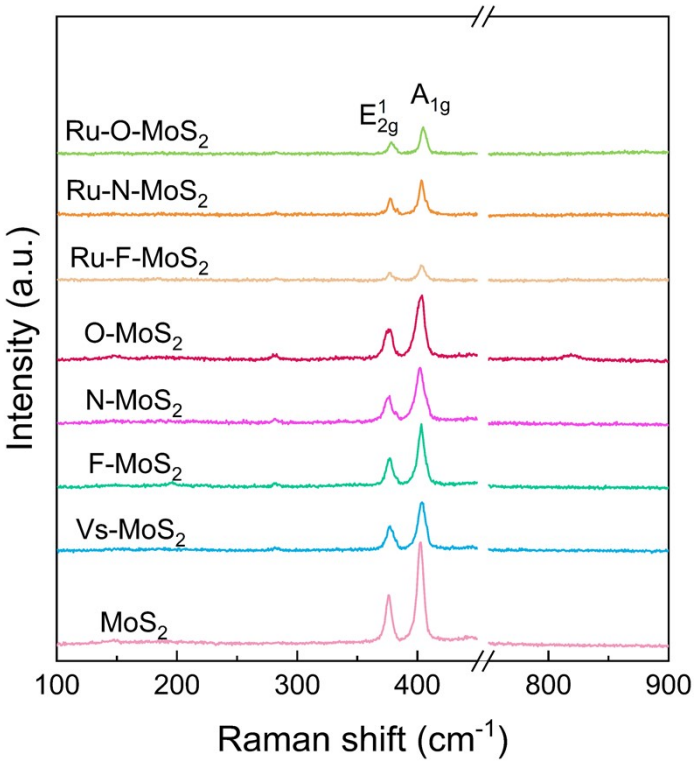

Figure S1. Raman spectra of pure MoS_2, Vs - MoS_2, F - MoS_2, N - MoS_2, O - MoS_2, Ru - F - MoS_2, Ru - N - MoS_2 and Ru - O - MoS_2.

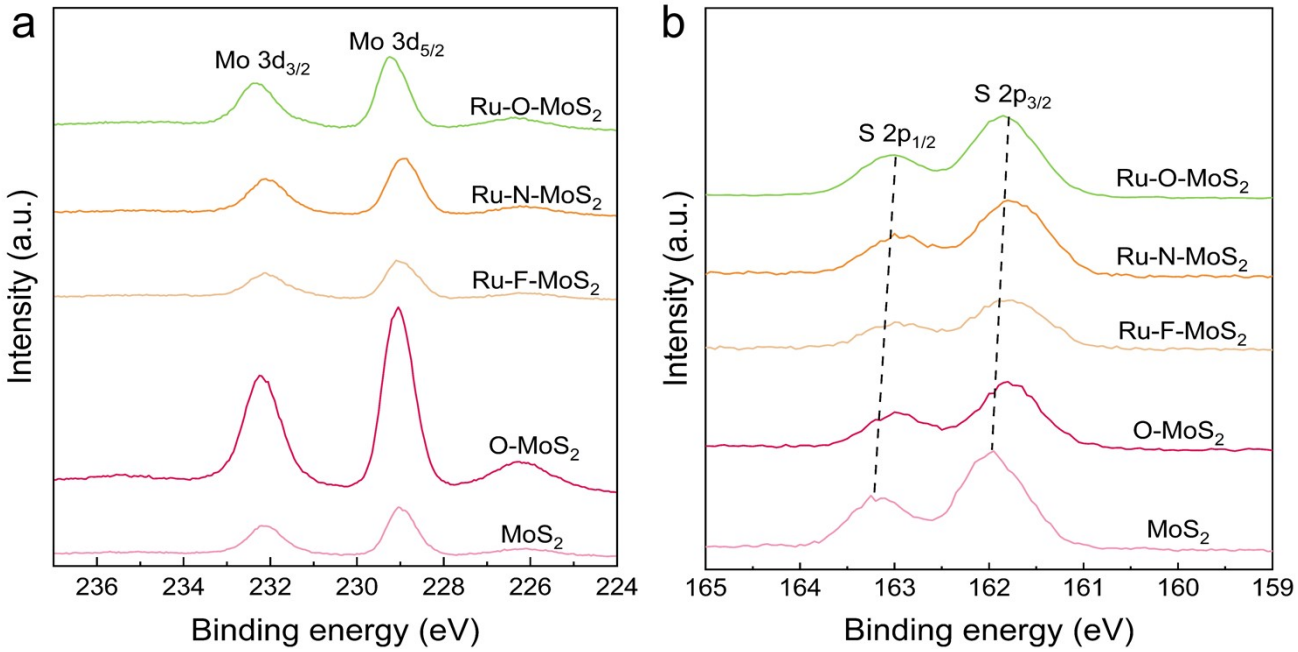

Figure S2. (a) Mo 3d peaks and (b) S 2p peaks pure MoS_2, O - MoS_2, Ru - F - MoS_2, Ru - N - MoS_2 and Ru - O - MoS_2 according to XPS data.

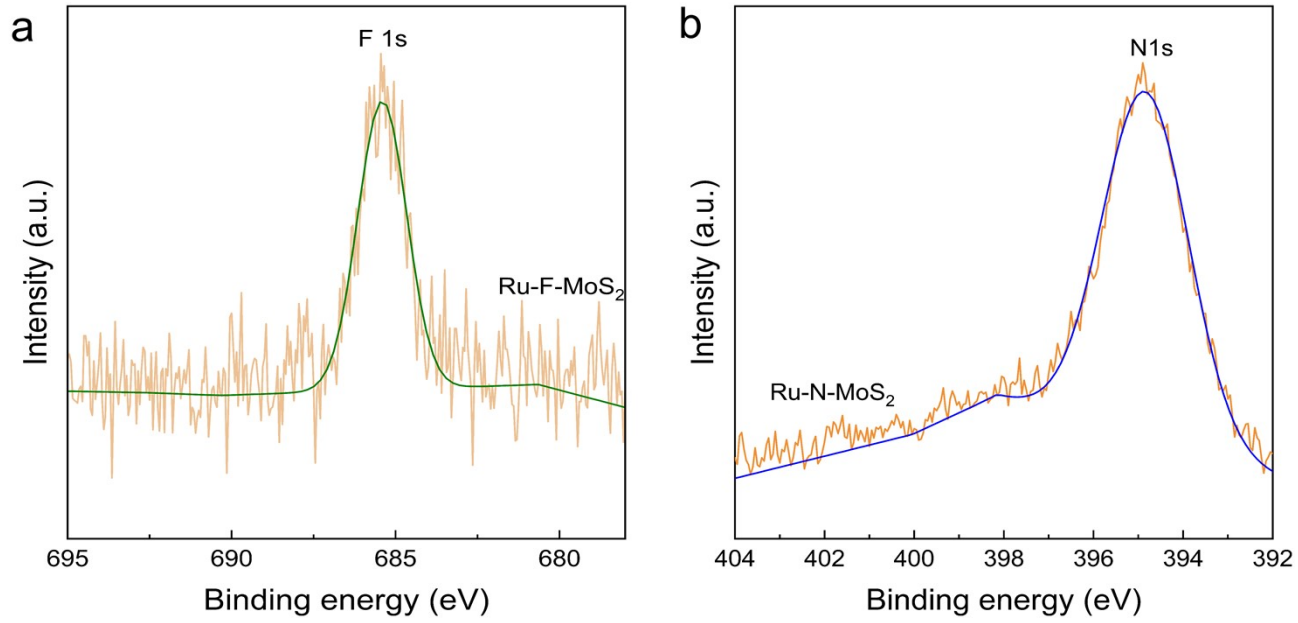

Figure S3. (a) F 1s peak Ru - F - MoS_2 and (b) N 1s peak of Ru - N - MoS_2 according to XPS data.

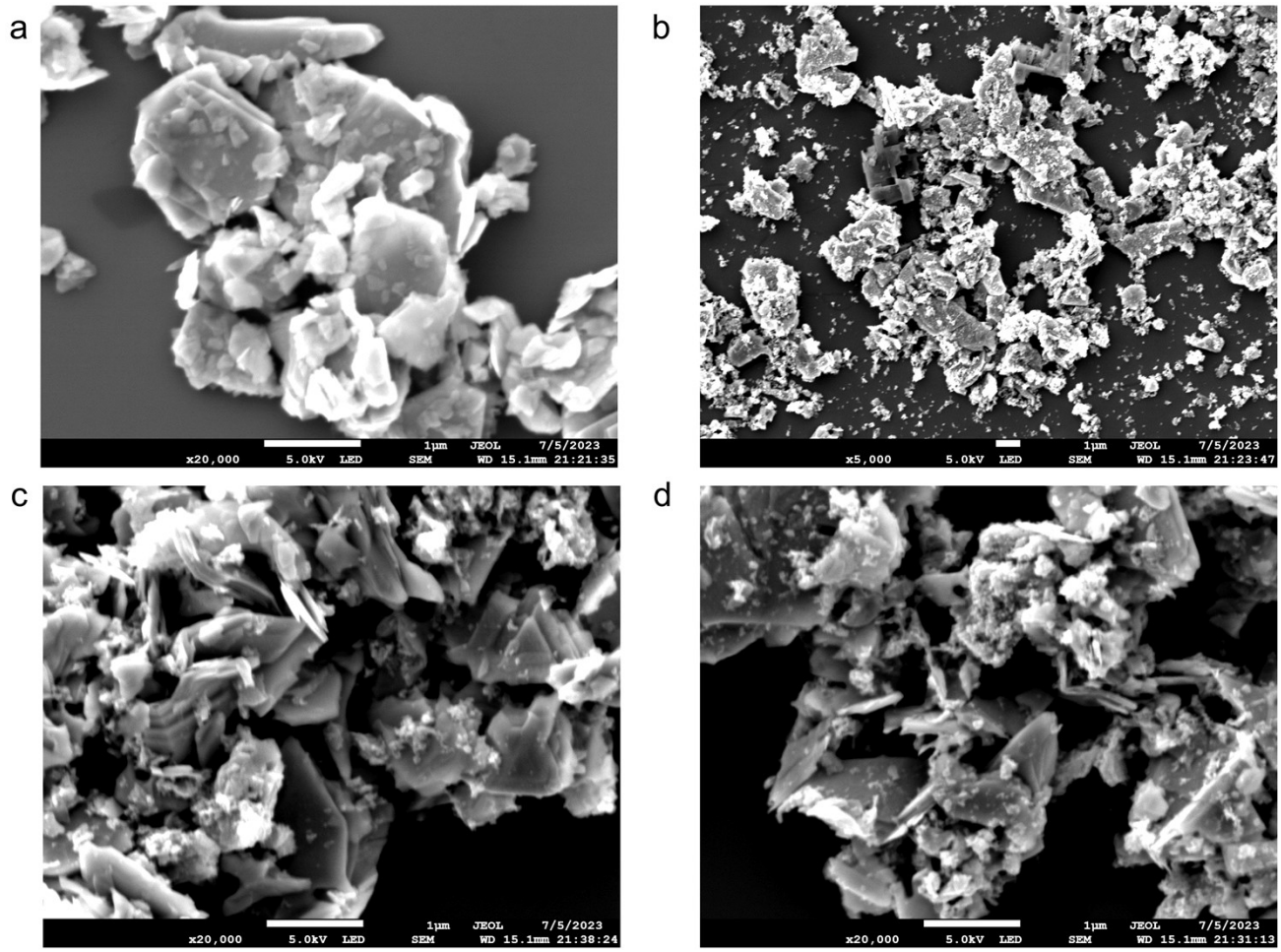

Figure S4. SEM images of (a) pure MoS_2, (b) Ru - F - MoS_2, (c) Ru - N - MoS_2 and (d) Ru - O - MoS_2.

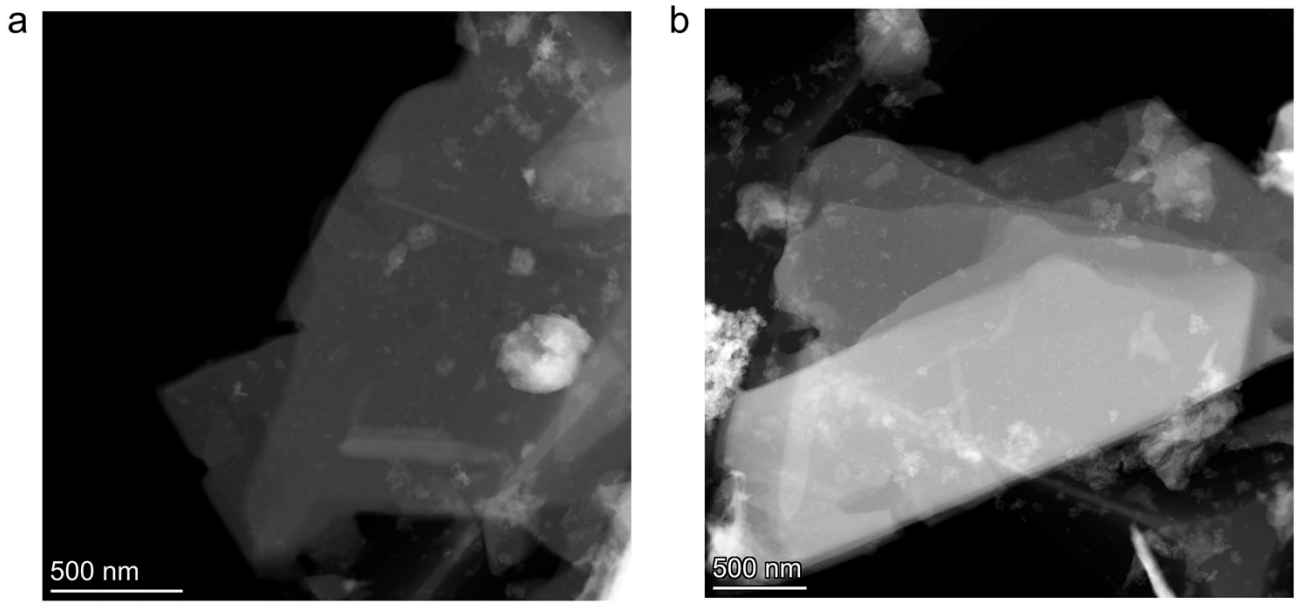

Figure S5. (a, b) STEM images of Ru - O - MoS_2 at low magnification.

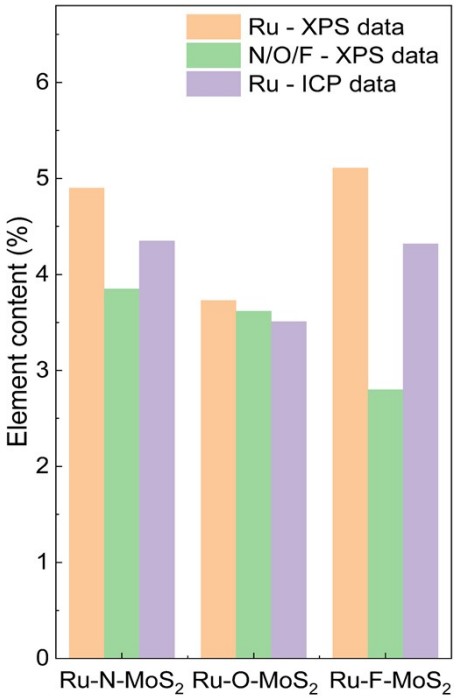

Figure S6. The content of Ru atom and nonmetallic atoms (N, O, F) in Ru - F - MoS_2, Ru - N - MoS_2 and Ru - O - MoS_2 based on ICP and XPS data.

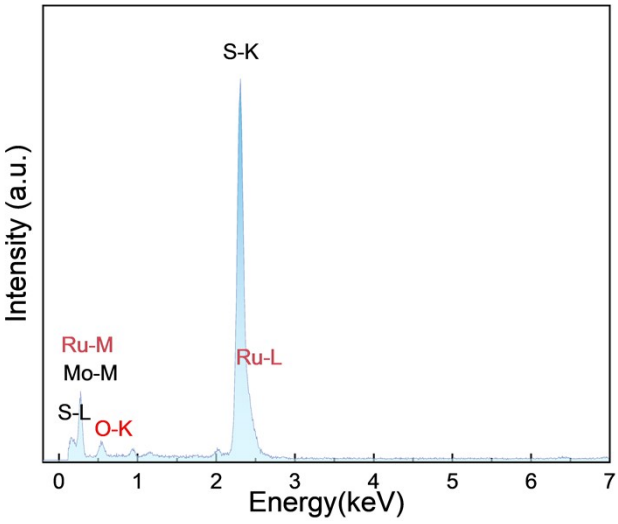

Figure S7. EDS spectra of Ru - O - MoS_2 nanosheets.

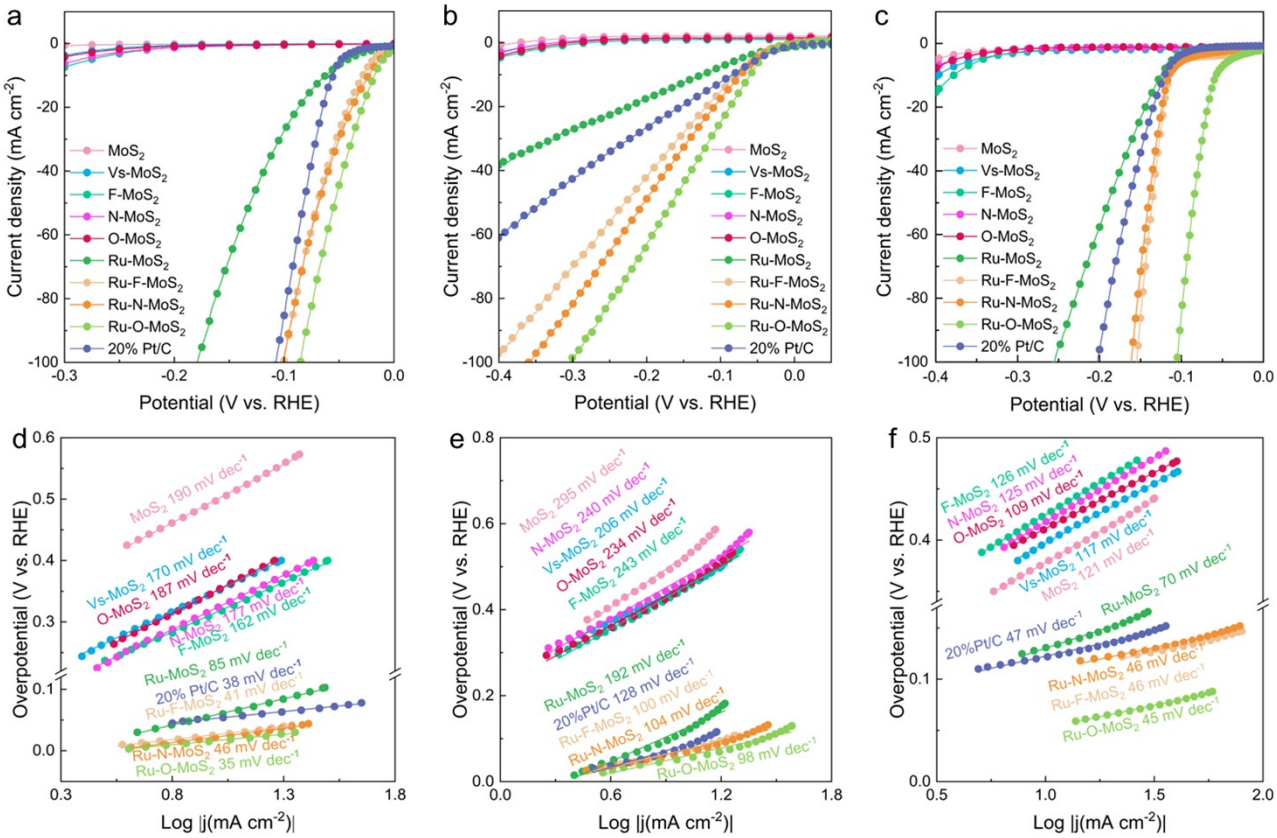

Figure S8. Electrocatalytic activity of as-prepared catalysts. HER Polarization curves of pure MoS_2, Vs - MoS_2, F - MoS_2, N - MoS_2, O - MoS_2, Ru - F - MoS_2, Ru - N - MoS_2 and Ru - O - MoS_2

electrocatalysts in (a) acidic, (b) neutral and (c) alkaline electrolytes. Tafel slope of pure MoS_2, Vs - MoS_2, F - MoS_2, N - MoS_2, O - MoS_2, Ru - F - MoS_2, Ru - N - MoS_2 and Ru - O - MoS_2 electrocatalysts in (d) acidic, (e) neutral and (f) alkaline electrolytes based on the polarization curve.

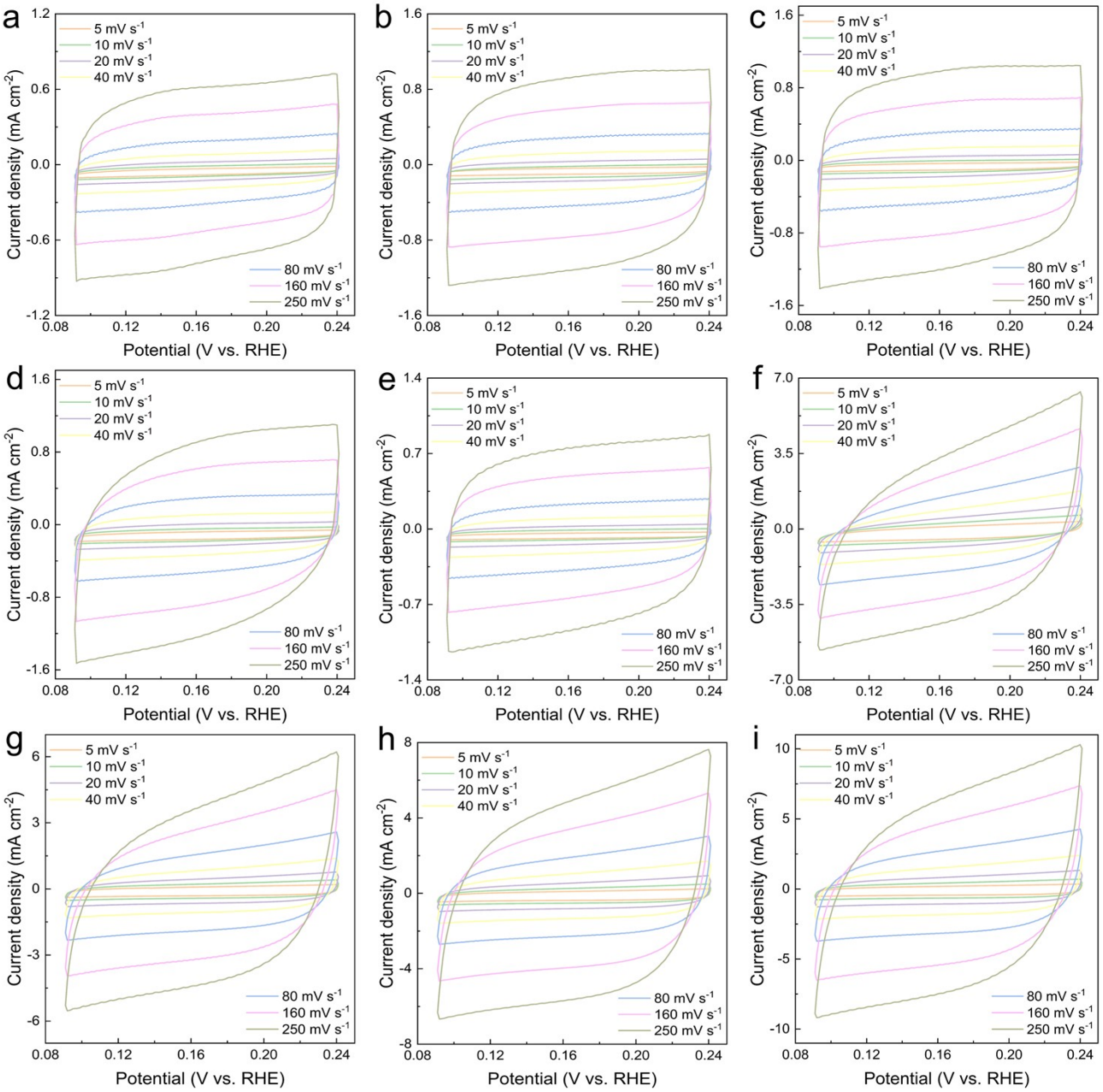

Figure S9. CV curves of samples in acidic electrolyte. (a) MoS_2, (b) Vs - MoS_2, (c) F - MoS_2, (d) N - MoS_2, (e) O - MoS_2, (f) Ru - MoS_2, (g) Ru - F - MoS_2, (h) Ru - N - MoS_2, (i) Ru - O - MoS_2.

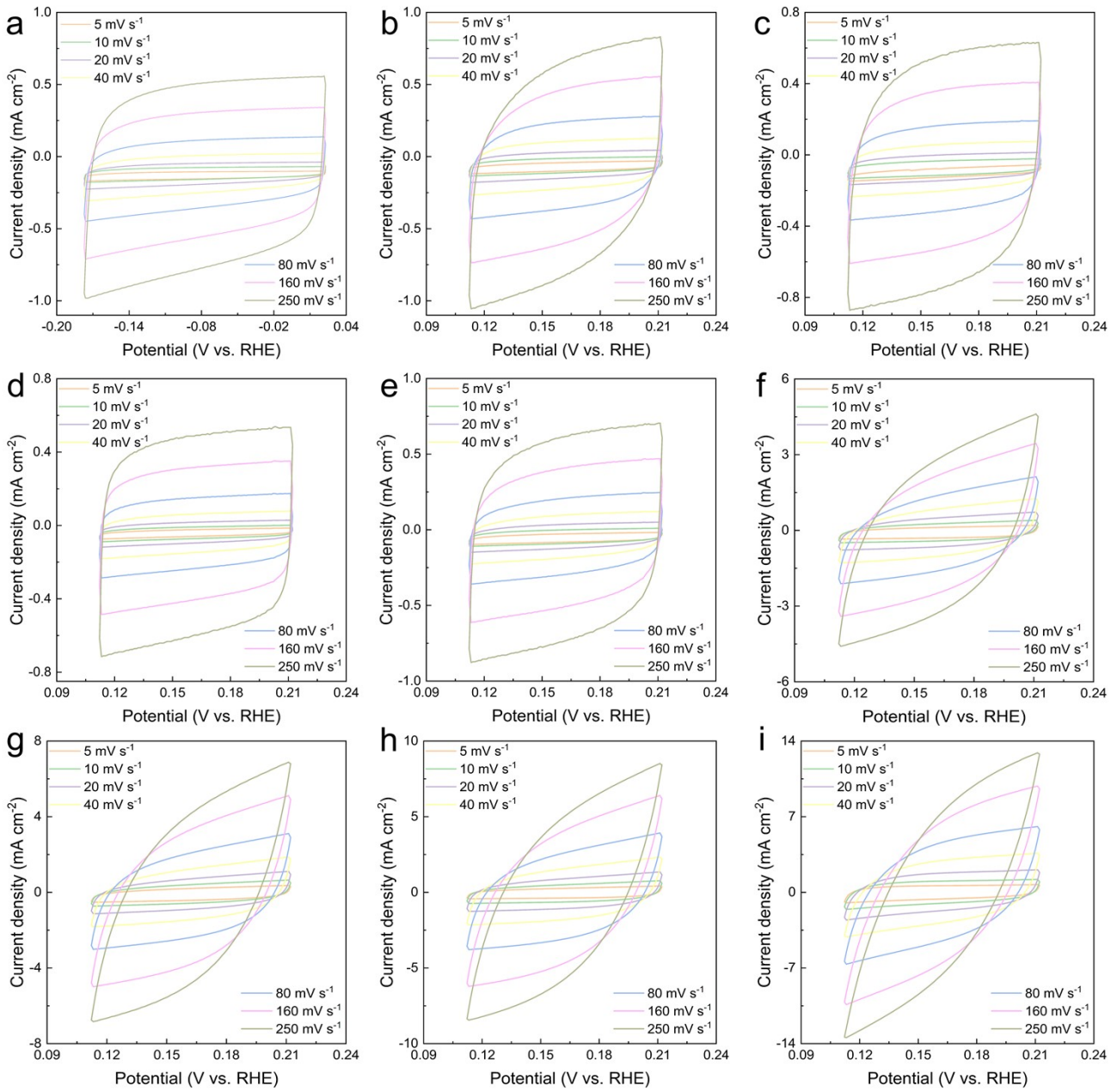

Figure S10. CV curves of samples in neutral electrolyte. (a) MoS_2, (b) Vs - MoS_2, (c) F - MoS_2, (d) N - MoS_2, (e) O - MoS_2, (f) Ru - MoS_2, (g) Ru - F - MoS_2, (h) Ru - N - MoS_2, (i) Ru - O - MoS_2.

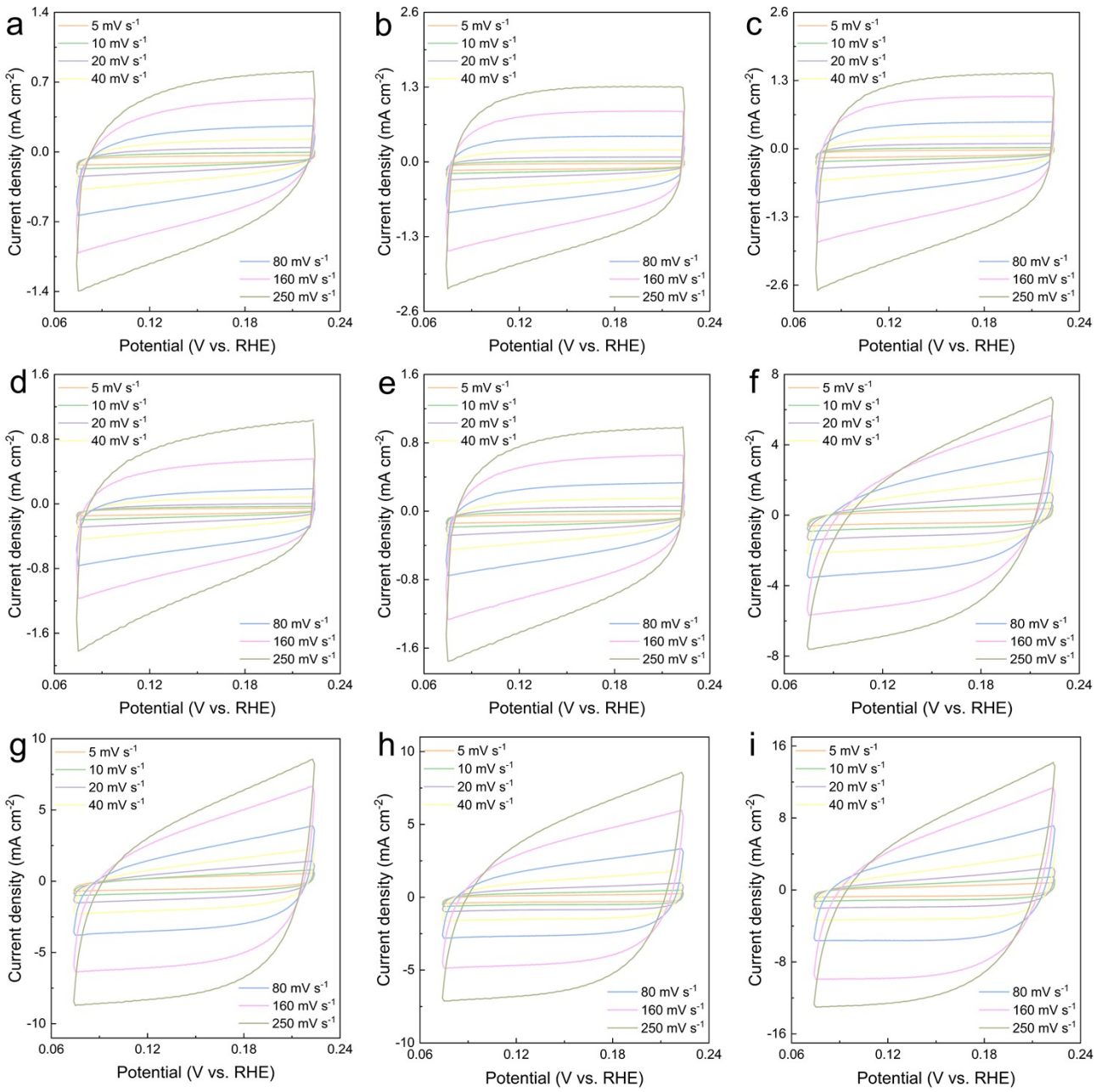

Figure S11. CV curves of samples in alkaline electrolytes. (a) MoS_2, (b) Vs - MoS_2, (c) F - MoS_2, (d) N - MoS_2, (e) O - MoS_2, (f) Ru - MoS_2, (g) Ru - F - MoS_2, (h) Ru - N - MoS_2, (i) Ru - O - MoS_2.

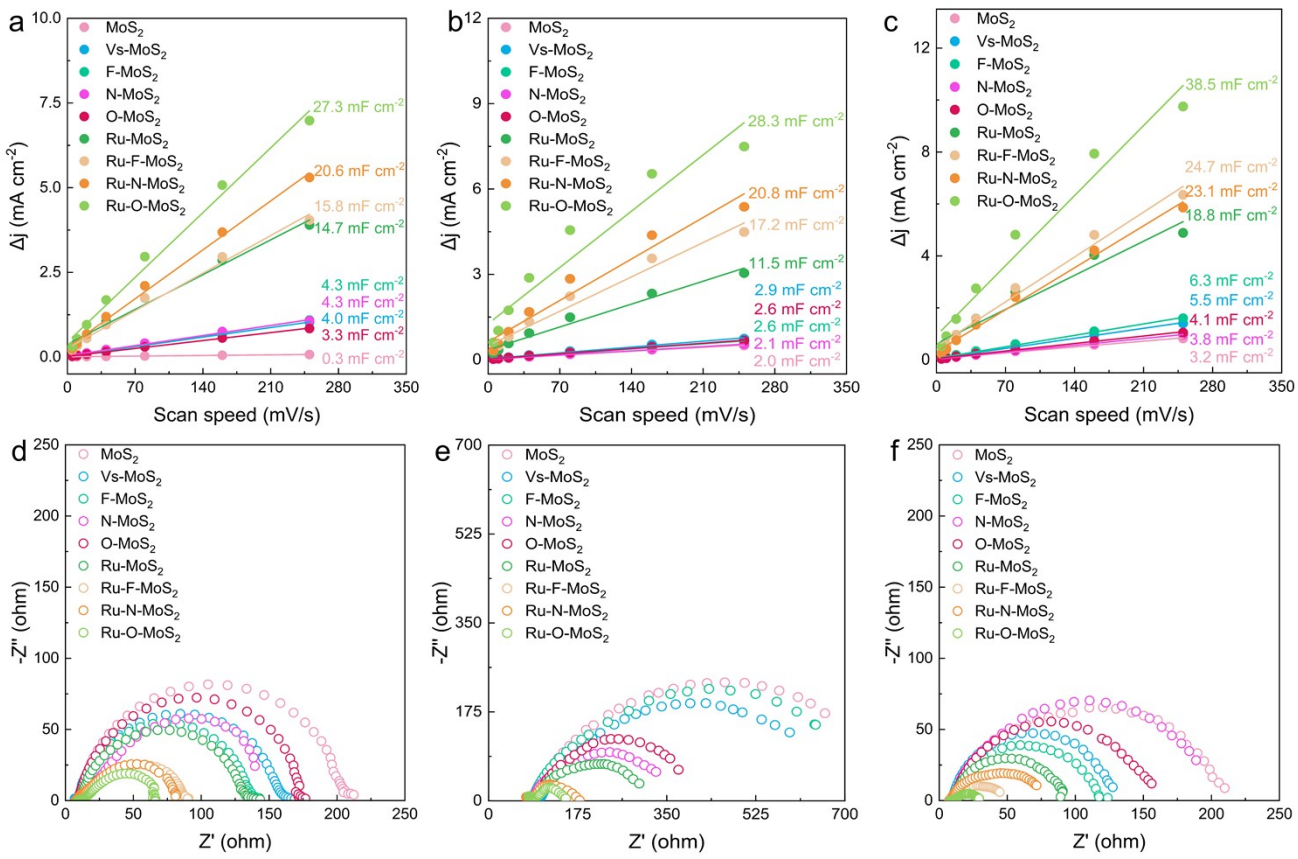

Figure S12. Electrochemical measurements of the as-prepared catalysts. Double layer capacitance of pure MoS_2, Vs - MoS_2, F - MoS_2, N - MoS_2, O - MoS_2, Ru - F - MoS_2, Ru - N - MoS_2 and Ru - O - MoS_2 electrocatalysts in acid (a), neutral (b), alkaline (c) electrolytes, respectively. Electrochemical impedance spectroscopy Nyquist plots of pure MoS_2, Vs - MoS_2, F - MoS_2, N - MoS_2, O - MoS_2, Ru - F - MoS_2, Ru - N - MoS_2 and Ru - O - MoS_2 electrocatalysts in acid (d), neutral (e), alkaline (f) electrolytes, respectively.

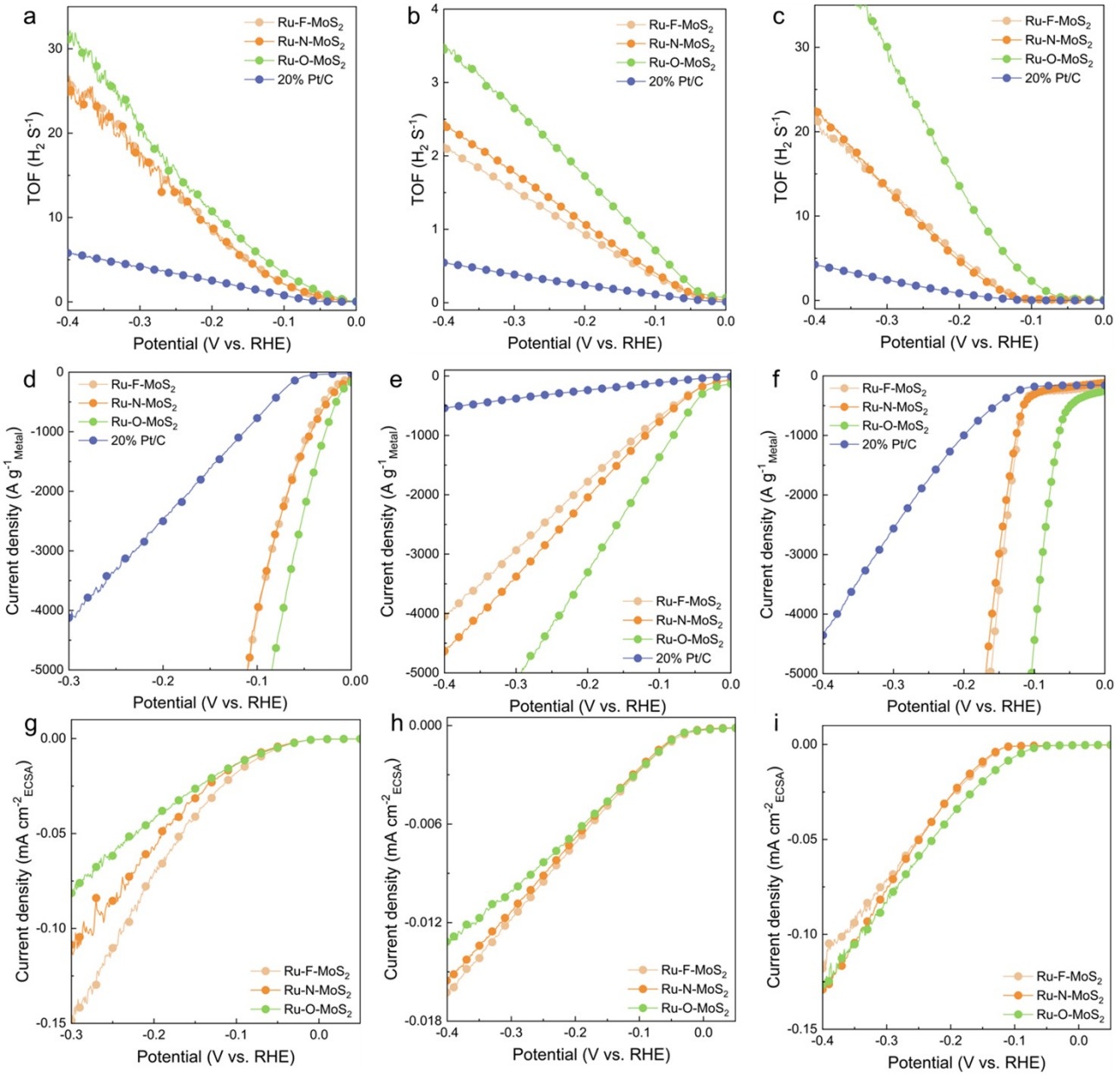

Figure S13. Turn over frequency (TOF) of catalysts in acidic (a), neutral (b) and alkaline (c) electrolytes; Mass activities of catalysts in acidic (d), neutral (e) and alkaline (f) electrolytes; Specific activities of the catalysts in acidic (g), neutral (h) and alkaline (i) electrolytes.

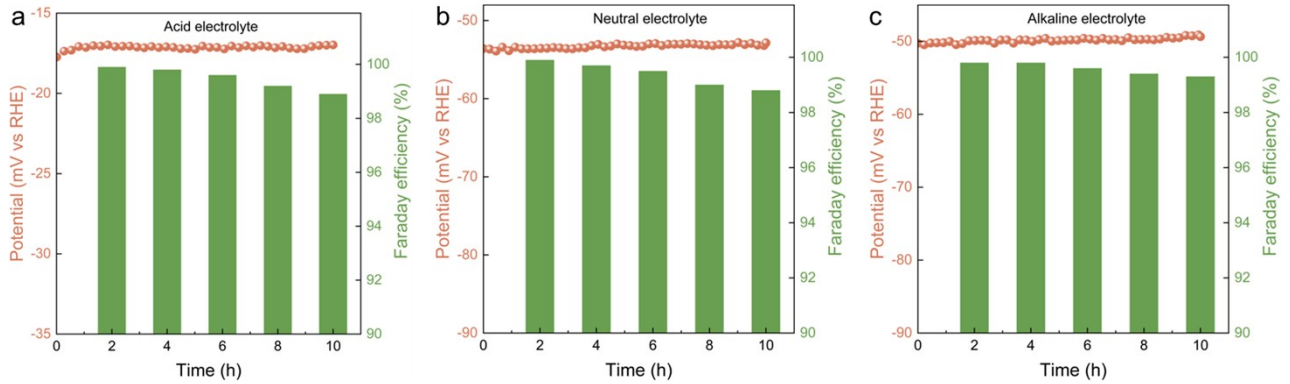

Figure S14. Faraday efficiency of the Ru-O-MoS_2 catalyst in acidic (a), neutral (b), alkaline (c) electrolytes.

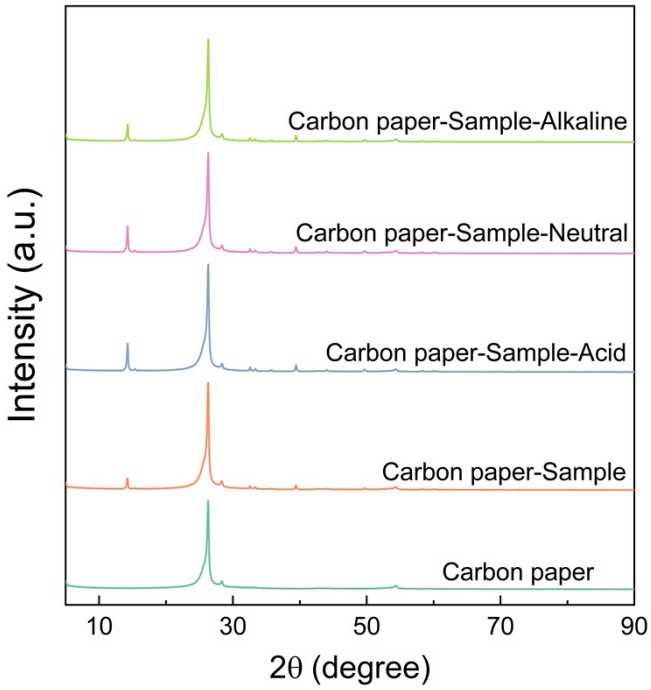

Figure S15. XRD of Ru-O-MoS_2 catalysts after stability tests in acidic, neutral and alkaline electrolytes for 60 h (samples were tested on carbon paper).

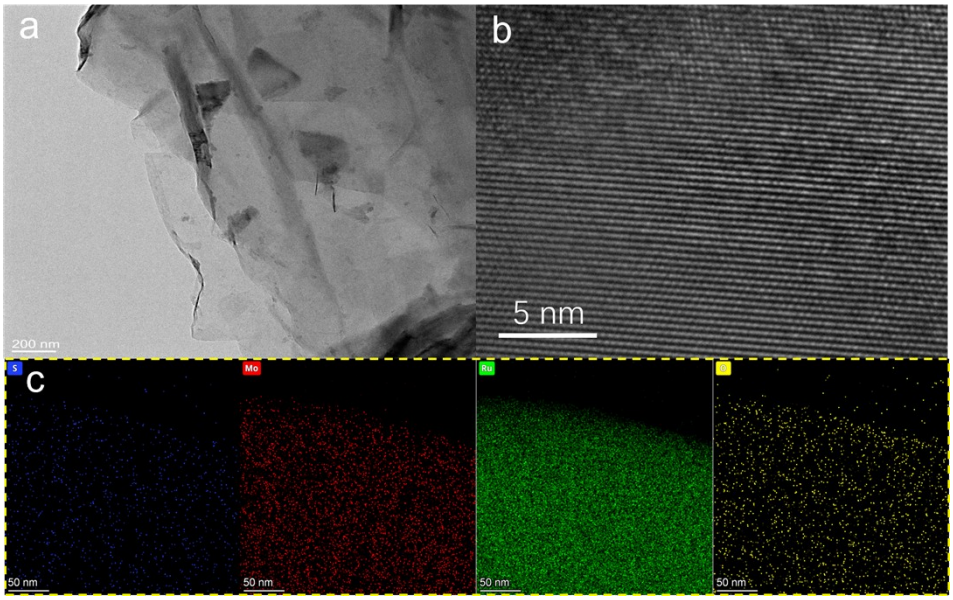

Figure S16. TEM (a, b) and EDS mapping images (c) of Ru-O-MoS_2 catalyst after stability tests in an acid electrolyte for 60 h.

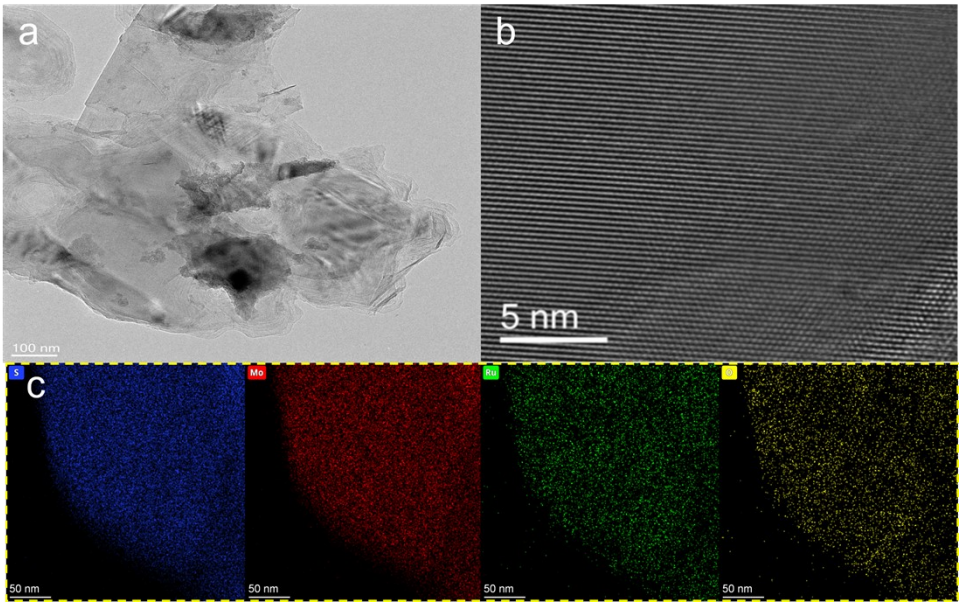

Figure S17. TEM (a, b) and EDS mapping images (c) of Ru-O-MoS_2 catalyst after stability tests in a neutral electrolyte for 60 h.

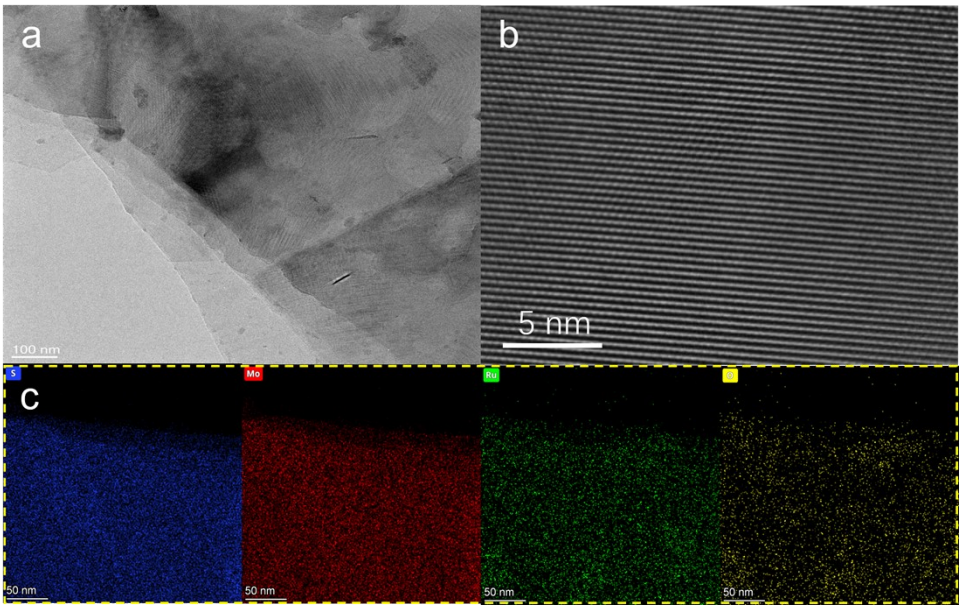

Figure S18. TEM (a, b) and EDS mapping images (c) of Ru-O-MoS_2 catalyst after stability tests in an alkaline electrolyte for 60 h.

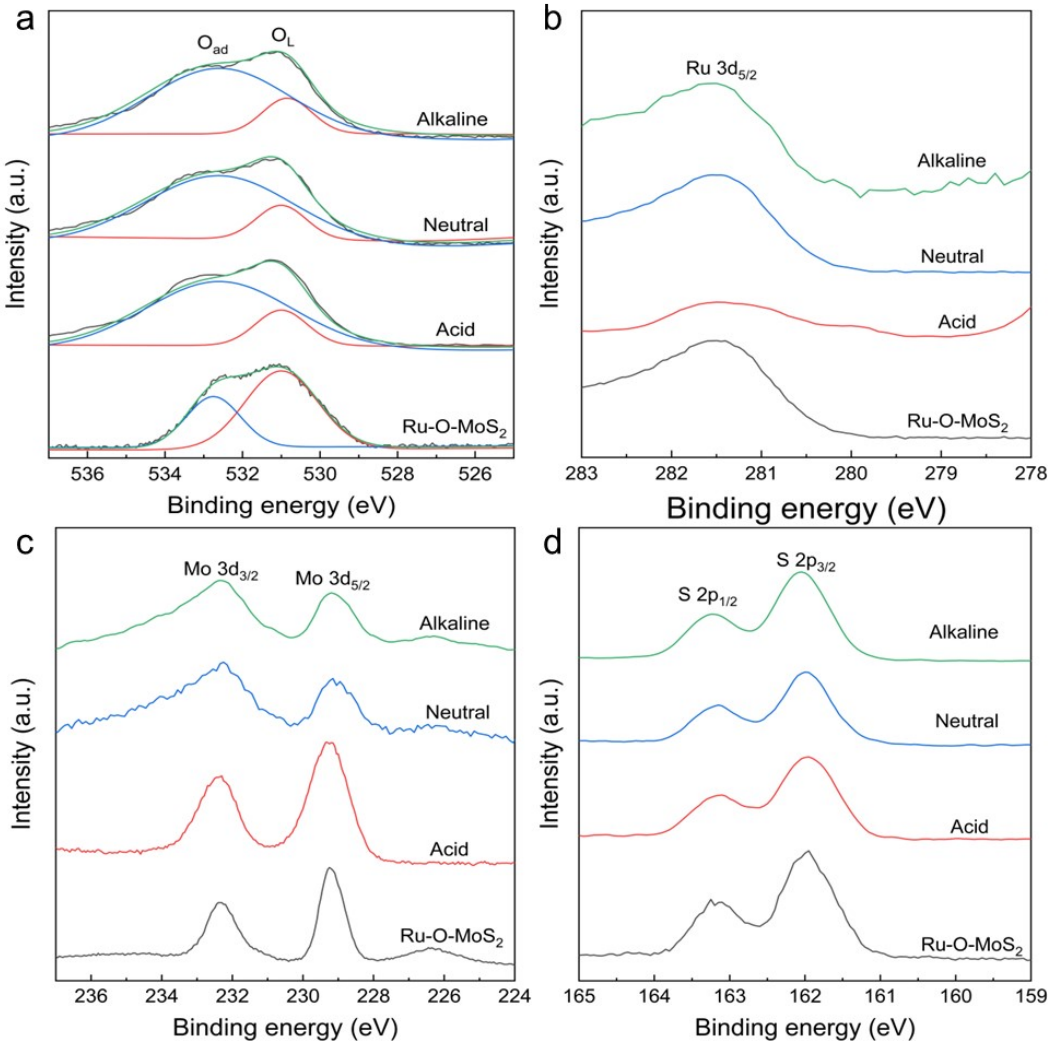

Figure S19. XPS comparison of Ru-O-MoS_2 catalyst after stability tests in acidic, neutral and alkaline electrolytes for 60 h with the Ru-O-MoS_2 catalyst before the reaction, which includes O 1s peaks (a), Ru 3d peaks (b), Mo 3d peaks (c) and S 2p peaks (d).

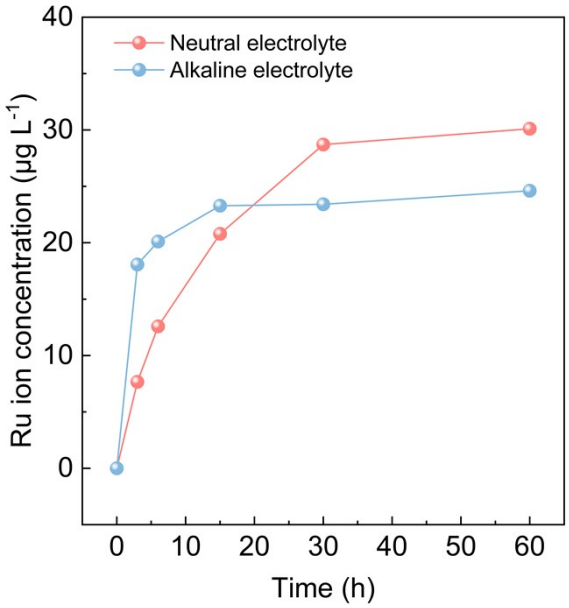

Figure S20. Ru ion concentration changes in neutral and alkaline electrolytes during stability testing of the Ru-O-MoS_2 catalyst.

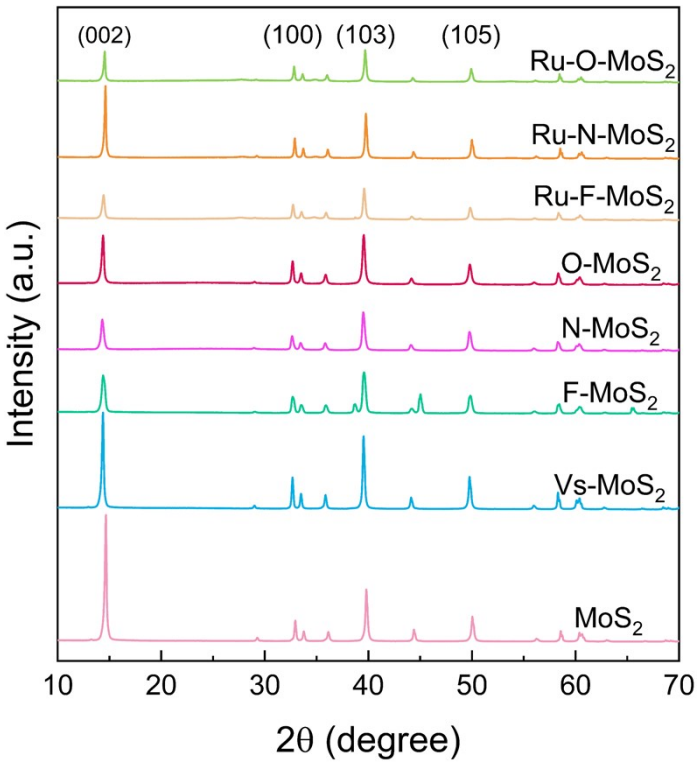

Figure S21. XRD data of pure MoS_2, Vs - MoS_2, F - MoS_2, N - MoS_2, O - MoS_2, Ru - F - MoS_2, Ru - N - MoS_2 and Ru - O - MoS_2.

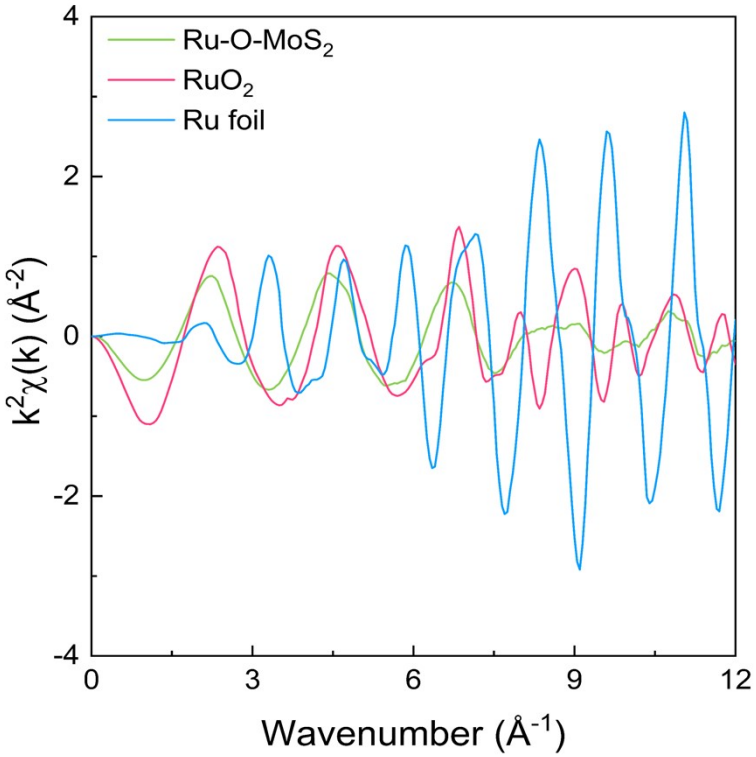

Figure S22. k^2-weighted $\chi(k)$-function of the EXAFS spectra for Ru K-edge.

Table S1. Overpotential and Tafel slop of the catalysts in 0.5 M H_2SO_4 electrolyte.

Catalysts	**η (mV) j=10 mV/cm²**	**Tafel slop (mV/dec^{-1})**
MoS_2	499	190
Vs-MoS_2	351	170
F-MoS_2	315	162
N-MoS_2	323	177
O-MoS_2	352	187
Ru-MoS_2	58	85
Ru-F-MoS_2	26	41
Ru-N-MoS_2	22	46
Ru-O-MoS_2	16	35
20% Pt/C	53	38

Table S2. Overpotential and Tafel slop of the catalysts in 1 M PBS electrolyte.

Catalysts	**η (mV) j=10 mV/cm²**	**Tafel slop (mV/dec⁻¹)**
MoS_2	518	295
Vs-MoS_2	454	206
F-MoS_2	448	243
N-MoS_2	466	240
O-MoS_2	452	234
Ru-MoS_2	116	192
Ru-F-MoS_2	71	100
Ru-N-MoS_2	67	104
Ru-O-MoS_2	54	98
20% Pt/C	80	128

Table S3. Overpotential and Tafel slop of the catalysts in 1 M KOH electrolyte.

Catalysts	**η (mV) j=10 mV/cm²**	**Tafel slop (mV/dec⁻¹)**
MoS_2	438	121
Vs-MoS_2	397	117
F-MoS_2	378	126
N-MoS_2	418	125
O-MoS_2	411	109
Ru-MoS_2	123	70
Ru-F-MoS_2	112	46
Ru-N-MoS_2	111	46
Ru-O-MoS_2	50	45
20% Pt/C	122	47

Table S4. HER performance of recently reported MoS_2-based catalysts in 0.5 M H_2SO_4 electrolyte.

Catalysts	**η (mV) j =10mV cm^{-2}**	**Tafel slop (mV dec^{-1})**	**Ref.**
Ru-O-MoS_2	16	35	This work
$Ru_{0.10}$@2H-MoS_2	168	78	[36]
$MSOR_1$	197	76	[37]
MoS2-1:4	84	69	[38]
1T'-MoS_2	149	42	[39]
Frenkel-defect MoS_2	164	36	[40]
Defect-rich 1T- MoS_2	136	45	[41]
M-MoS_2	210	61	[42]
Pt@MoS_2	88	56	[43]
rGO-CNT/MoS_2	88	31	[44]
Se-MoS_2 (1T)	108	47	[45]
MoS_2-Ti_3C_2(1T')	163	45	[46]
CN/CNL/MoS_2/CP(1 T/2H)	112	77	[47]
$V_{0.05}Mo_{0.95}S_2$ (1T)	156	54	[48]
1T-2H MoS_2/N-rGO	97	39	[49]
C_{ia}-MoS_2	87	45	[50]
1%Ce-ReS_2	306	99	[51]

Table S5. Curve fit parameters of Ru k-edge EXAFS for Ru - O - MoS_2.

Sample	Path	N	R (Å)	σ^2 (10^{-3} Å^2)	R-factor
Ru-O-MoS_2	Ru-O	1.9±0.2	1.99±0.01	4.5	0.008
	Ru-S	1.1±0.3	2.21±0.05	7.5	
	Ru-Mo	0.3±0.1	2.70±0.01	1.3	

In the context of our fitting, several key parameters were meticulously defined and refined to ensure the accuracy and reliability of our findings. The amplitude reduction factor, denoted as S_0^2, was a fixed parameter set at 0.8. The edge-energy shift, represented by ΔE_0, played a crucial role in our analysis. It signified the difference between the zero kinetic energy value of the sample and that of the theoretical model. Through a comprehensive global fit, this parameter was refined, yielding a specific value of -7.5 eV. Our data were acquired within specific ranges: $3 \leq k \leq 12.2$ Å^{-1} and $1 \leq R \leq 2.7$ Å. Here, k denoted the wave vector magnitude, and R represented the interatomic distance, capturing the bond length between central atoms and surrounding coordination atoms. The coordination number (N) was a crucial aspect of our analysis, providing insights into the arrangement and organization of atoms within the material. The interatomic distance (R) not only contributed to the coordination number calculation but also served as a fundamental parameter in understanding the structural aspects of the material. Additionally, the Debye-Waller factor (σ^2) played a pivotal role, serving as a measure of thermal and static disorder in absorber-scatter distances. Additionally, the Debye-Waller factor (σ^2) played a pivotal role, serving as a measure of thermal and static disorder in absorber-scatter distances. To assess the overall quality of our fitting, we employed the R-factor. This parameter served as a valuable metric, quantifying the goodness of

the fitting.

References

(1) Ravel, B.; Newville, M., ATHENA, ARTEMIS, HEPHAESTUS: data analysis for X-ray absorption spectroscopy using IFEFFIT. *J. Synchrotron. Radiat* **2005,** *12* (4), 537-541.

(2) Anjum, M. A. R.; Lee, J. S., Sulfur and nitrogen dual-doped molybdenum phosphide nanocrystallites as an active and stable hydrogen evolution reaction electrocatalyst in acidic and alkaline media. *ACS Catal.* **2017,** *7* (4), 3030-3038.

(3) Anjum, M. A. R.; Jeong, H. Y.; Lee, M. H.; Shin, H. S.; Lee, J. S., Efficient hydrogen evolution reaction catalysis in alkaline media by all-in-one MoS_2 with multifunctional active sites. *Adv. Mater.* **2018,** *30* (20), 1707105.

(4) Greeley, J.; Jaramillo, T. F.; Bonde, J.; Chorkendorff, I.; Nørskov, J. K., Computational high-throughput screening of electrocatalytic materials for hydrogen evolution. *Nat. Mater.* **2006,** *5* (11), 909-913.

(5) Nørskov, J. K.; Bligaard, T.; Logadottir, A.; Kitchin, J. R.; Chen, J. G.; Pandelov, S.; Stimming, U., Trends in the exchange current for hydrogen evolution. *J. Electrochem. Soc.* **2005,** *152* (3), J23.

(6) Perdew, J. P.; Burke, K.; Ernzerhof, M., Generalized gradient approximation made simple. *Phys. Rev. Lett.* **1996,** *77* (18), 3865.

(7) Kresse, G.; Furthmüller, J., Efficiency of ab-initio total energy calculations for metals and semiconductors using a plane-wave basis set. *Comp. Mater. Sci.* **1996,** *6* (1), 15-50.

(8) Kresse, G.; Furthmüller, J., Efficient iterative schemes for ab initio total-energy calculations using a plane-wave basis set. *Phys. Rev. B Condens Matter* **1996,** *54* (16), 11169.